Trans. Tianjin Univ. (2018) 24:51–58
https://doi.org/10.1007/s12209-017-0081-y

RESEARCH ARTICLE

Numerical Study on Helical Fiber Fragmentation in Chiral Biological Materials

Jianshan Wang[1] · Li Yuan[1] · Lixin Wang[2] · Yuhong Cui[1] · Qinghua Qin[3]

Received: 15 January 2017 / Revised: 21 March 2017 / Accepted: 20 April 2017 / Published online: 28 August 2017

Abstract Chiral microstructures exist widely in natural biological materials such as wood, bone, and climbing tendrils. The helical shape of such microstructures plays an important role in stress transfer between fiber and matrix, and in the mechanical properties of biological materials. In this paper, helical fiber fragmentation behavior is studied numerically using the finite-element method (FEM), and then, the effects of helical shape on fiber deformation and fracture, and the corresponding mechanical mechanisms are investigated. The results demonstrate that, to a large degree, the initial microfibril angle (MFA) determines the elastic deformation and fracture behavior of fibers. For fibers with a large MFA, the interfacial area usually has large values, inducing a relatively low fragment density during fiber fragmentation. This work may be helpful in understanding the relationship between microstructure and mechanical property in biological materials, and in the design and fabrication of bio-inspired advanced functional materials.

Keywords Chiral biological materials · Helical fiber · Fiber fragmentation · Deformation · Dissipated energy

✉ Jianshan Wang
wangjs@tju.edu.cn

[1] Department of Mechanics, Tianjin University, Tianjin 300054, China

[2] China Automotive Technology and Research Center, Tianjin 300300, China

[3] Research School of Engineering, Australian National University, Canberra ACT 0200, Australia

Introduction

To adapt themselves to various environmental conditions, natural biological materials often exhibit remarkable mechanical properties, such as superior toughness, strength, and elasticity [1]. Well-known examples include wood, bone, shell nacre, teeth, and spider silk. These high-performance and optimized biological materials are generally made up of relatively weak components, such as brittle inorganic minerals, soft proteins, and celluloses. Through their intricate multi-scale and multi-functional microstructures, they achieve an increase in mechanical properties by several orders of magnitude higher than values predicted from a simple mixture of such composites. This natural formation principle can be transferred to the material science and engineering fields to provide high strength and toughness for the next generation of advanced functional bio-materials. Therefore, understanding the structure/property relationship of biological materials has been a promising challenge in past decades.

As a result of a series of structural evolutions and the optimization of their chemical, physical, and biological components, a great diversity of micro- and nano-structures with defined shape and size, such as the bricks-and-mortar-like microstructure of nacres, have been produced in most biological materials [1–6]. These elaborate micro- and nano-structures endow biological materials with highly integrated properties or functions such as toughness, elasticity, density, and permeability, and enable them to reach a perfect compromise between different properties and functions. Among naturally developed micro- and nano-structures, chiral microstructures may be the most pervasive as they exist at almost every structural level in many different forms of biological material [7–10]. For example, the cellulose fibril winds helically in most plant cell walls

and the collagen filament also takes a helical shape in tendons, ligaments, bone, and so on. Biological microstructures taking chiral forms such as helical and twisted are regarded as a unified structural principle that biological materials should obey during the biomineralization process or biopolymer assembly [9, 11, 12]. In general, there are several representative structural forms of chiral microstructure in animal and plant organs and tissues. One typical form is the micro- and nano-scale cellulose or collagen helix embedded in the building block elements of biological materials consisting of hemicellulose and a lignin matrix, or in mineral lamellae [13]. Wood, bone, and towel gourd tendrils are some typical examples. Another is a chiral stack structure, such as the Bouligand structure in crab exoskeletons, which is composed of a helical or twisted arrangement of fibrils or rods [1]. In addition, in many soft tissues such as tendons and ligaments, collagen fibrils wind around each other, forming a rope structure. In some biological materials such as towel gourd tendrils, the chiral microstructures even form a hierarchy [6].

Due to their three-dimensional helical period shapes, chiral microstructures usually exhibit complicated deformation and internal force fields under applied loading. When stretched, they exhibit twisting, bending, and elongation, and a distinct coupling between twisting and elongation exists [14, 15]. Under low tensile strain, the twist-stretch coupling deformation is generally linear, while under high strain, this coupling relationship becomes nonlinear, depending on the material properties and helical geometry [7]. The corresponding stress fields exhibit complicated spatial distributions induced by deformation and coupling. When embedded in biological materials, chiral microstructures such as helical fibrils usually serve as reinforcing elements to transfer stress through interfaces. Furthermore, the large interfacial area induced by the helical geometry of chiral microstructures results in a high capacity for energy dissipation during failure, such as the interfacial debonding and frictional sliding during helical fiber pull-out [11]. In addition, the presence of chiral microstructures sometimes results in their composite exhibiting hardening-type nonlinear constitutive behavior, which can also induce a relatively high capacity for energy absorption during deformation and rupture [16]. A recent study demonstrated that wood cell walls undergo elastic, slip-stick plastic, and high-strain stiffening deformation when stretched, and that this is controlled by the helical winding of the cellulose fibrils [17]. Thus, biological materials with chiral microstructures often exhibit superior properties such as high elasticity and fracture toughness. For example, the fracture toughness of wood is about 20% higher than that predicted by the mixed law of a simple fibrous composite. This great difference in values is mainly attributed to the helical winding of cellulose fibril in the second layer of wood cell walls [8, 11].

In biological materials subjected to external loading, stress transfer through the interface between the chiral microstructures and matrix occurs. Here, the contained chiral microstructures, such as helical fibrils, are elongated as a result of an increase in helical shape size from deformation of the matrix [11]. When the deformation reaches a critical value, failure and nonlinear stress–strain behavior may occur, which helps the biological organs or tissues adapt to complicated environments. Different from the traditional fiber composites, the matrix of chiral biological composites consisting of biomacromolecules can generally endure large deformation. Due to the three-dimensional geometry and twist-stretch coupling deformation of a helical fiber, the stress transfer between the fiber and the matrix involves tangential and circumferential shear stress. These features of deformation and stress lead to much more complicated failure progress. Compared with the traditional fiber composites, the failure progress of biological materials or composites with helical fibrils and other chiral inclusions involves not only deformation and fracture of the microstructures and their interactions at multiple structural levels, but also complicated deformation and internal force fields induced by the uniform curvature and torsion of the chiral microstructures themselves [11]. Typical failure progress of biological composites with helical fibrils also includes helical fiber/matrix interfacial debonding, and helical fiber fracture and pull-out from the elastic matrix. The previous studies on the traditional fiber composites have extensively investigated these failure progresses [18–24]. Recently, Wang et al. [11] conducted an FEM simulation of the pull-out progress of a helical fiber from an elastic matrix in biological materials such as wood. The results showed that the displacement–force curves of helical fiber pull-out have a similar shape to those of a straight fiber. Due to its large interfacial area and helical geometry, the values of pull-out force and energy dissipation of a helical fiber composite are much higher than those of its straight counterpart. Fracture of chiral microstructures, such as helical fibers, also often occurs during the failure of biological composites and accounts for the high energy dissipation that plays an important role in achieving high toughness. For example, ligaments, tendons, and towel gourd tendrils can undergo large tensile deformation due to their helical fibrils, which themselves are often broken during large deformation.

However, how chiral microstructures affect the deformation and fracture of biological materials during the loading process has not yet been studied. In this paper, we conduct an FEM simulation to quantitatively investigate the fragmentation behavior of a helical fiber in a

hyperelastic matrix. We mainly focus on how the helical shape affects deformation and fracture of the fiber.

FEM Modeling of Helical Fiber-Matrix System

In this paper, the fiber-matrix system shown in Fig. 1 is considered representative of a chiral biological composite, in which a helical fiber is embedded in a cylindrical matrix. The matrix is generally made up of hemicellulose, polysaccharides, proteins, and other biomacromolecules. Thus, it can be taken as a hyperelastic material and can usually endure large deformation. The loading was applied to both ends of the matrix. During loading, stress transfer between the helical fiber and the matrix, and the shape of the helical fiber correspondingly change. Due to the three-dimensional helical geometry of the fiber, only the fiber helix is stretched, and the strain in the fiber stays small, even though the helical fiber-matrix system is undergoing large deformation. With an increase in applied loading, the fiber strain increases and it may even break, similar to the traditional fiber fragmentation behavior in composites.

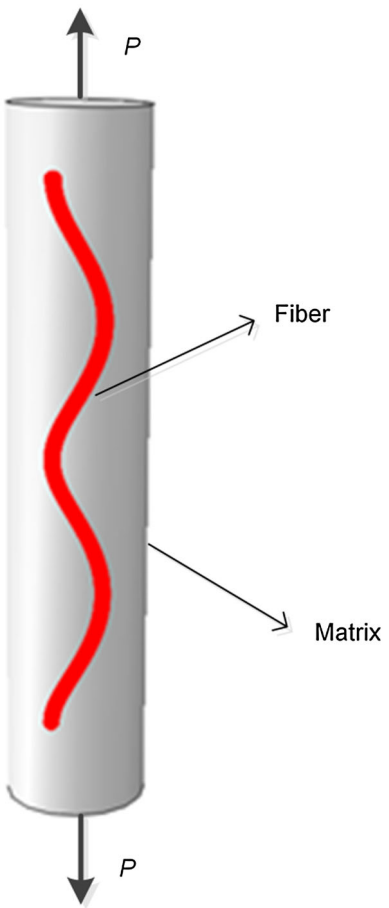

Fig. 1 Representative element of chiral biological materials

Here, we consider helical fiber fragmentation and mainly focus on the effects of helical shape on the deformation and fracture of biological materials. For simplicity, it is assumed that the fiber exhibits small elastic–plastic deformation.

The software ABAQUS was used to conduct the FEM simulation of the deformation and fracture behavior of fibers. In the simulation, the helical radius and length of fiber were $r = 15$ nm and $l = 1.2$ μm, respectively. The radius and length of the cylinder matrix were $R = 150$ nm and $L = 1.5$ μm, respectively. The mechanical behavior of the interface between the helical fiber and the matrix can be described by a cohesive model with a traditional bi-linear constitutive relationship. The maximum nominal stress criterion was taken as the interfacial debonding point. The property parameters of the interface elements were $G = 0.4$ J/m^2, $K = 500$ MPa, and $T_{\text{interface}} = 10$ μN, where $T_{\text{interface}}$ denotes the maximal nominal stress of the interface, G is the energy release rate, and K is the interfacial strength. The extensively used Mooney–Rivlin model was employed to simulate the mechanical behavior of the matrix. The polynomial strain potential energy model can be written as follows [25]:

$$U = C_{10}(\bar{I}_1 - 3) + C_{01}(\bar{I}_2 - 3), \quad (1)$$

where C_{10} and C_{01} are material parameters related to temperature; $\bar{I}_1$ and $\bar{I}_2$ are deviatoric strain invariants in terms of the principal stretches. C_{10} and C_{01} are assumed to be constant, and can be determined through the relations: $C_{10} = K_1 = NkT/2$ and $C_{01} = K_2/2$, where N denotes the average number of polymer chains per unit volume, k is the Boltzmann constant, and T is the absolute temperature, both K_1 and K_2 are constants. It was found that the value of C_{10} ranged from 1/10 to 1/4 of C_{01} only. In this paper, the matrix properties are similar to those of rubber, and we assume: $C_{10} = 0.1206$, $C_{01} = 0.4825$. Elastic–plastic fracture criterion was adopted for fiber breakage, and the elastic modulus and Poisson's ratio were taken as $E_f = 1.0$ GPa and $\nu_f = 0.4$, respectively. In the simulation, the force was applied to the matrix along its axial direction with a constant speed of 0.05 μm/s. It should be mentioned that similar simulation results can be obtained if the parameters involved take other reasonable values. Thus, the simulation in this paper is capable of capturing the main mechanical features of the fragmentation behavior of helical fibers in chiral biological materials.

Deformation of Helical Fiber-Matrix System

Under certain tensile loading, the helical fiber-matrix system may undergo large deformation and the fiber shape may experience distinct changes. In Fig. 2, configurations

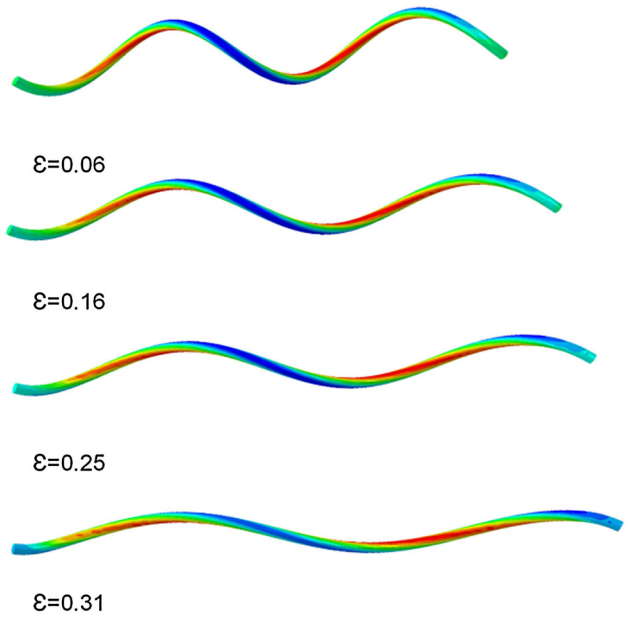

Fig. 2 Shape changes in helical fibers during the tensile testing of the fiber-matrix system with an initial MFA = 45°

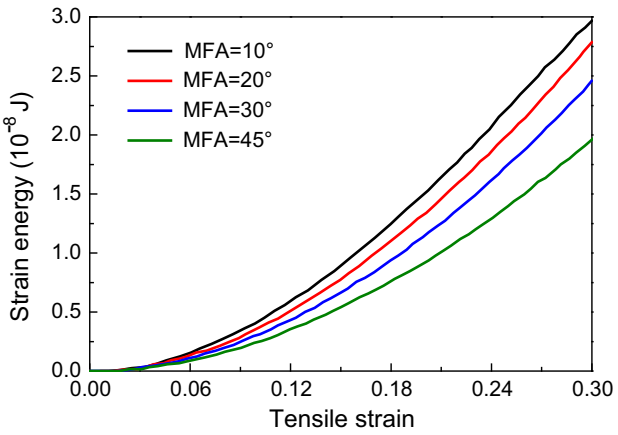

Fig. 3 Variations in strain energy of the fiber-matrix system with different MFAs under tensile strain

of helical fibers corresponding to tensile strains $\varepsilon = 0.06$, 0.16, 0.25, and 0.31 have been plotted to show the microstructure changes during the loading process. In the computation, the value of initial microfibril angle (MFA) was taken as 45°. The geometrical configuration of the helical fiber can be described by the helical angle and helical pitch. In the literature, MFA is often used to describe the shape of cellulose fibrils as they helically wind on plant cell walls. MFA is defined as the angle between an inclined cellulose fibril and the central axis of a cell wall. The value of MFA ranges from 0° to 90°. The sum of the MFA and the helical angle equals 90°. To maintain consistency, MFA is used here to describe the helical shape of a fiber. During the loading process, the fiber helix was stretched under the action of shear stress and simultaneously twisted with a decrease in MFA. Recent study shows that if the initial value of MFA is smaller than 45°, the fiber helix is usually twisted with the decrease in MFA, and its degree of twist increases [7]. When the value of MFA equals 45°, the degree of twist reaches its maximum. After this, the fiber helix is twisted in the reverse direction and its degree of twist decreases. In addition, shape changes to the fiber helix occur during tensile testing and the fiber strain stays small, even when the tensile strain reaches 0.20.

If interfacial debonding and fiber breakage are not considered, the work done by the applied loading is mainly stored in the fiber-matrix system in the form of strain energy. Figure 3 shows the variation in strain energy of the fiber-matrix system with matrix deformation for different initial MFAs. It can be seen that the strain energy of the fiber-matrix system increases nonlinearly with an increase in tensile strain. For fiber-matrix systems with relatively large initial MFA values, the strain energy mainly comes from tensile deformation of the matrix and the bending and twisting deformation of the fiber helix induced by shape changes, while the axial deformation of the fiber stays small. For a fiber-matrix system with a relatively small initial MFA, the axial deformation increases and cannot be neglected. In this case, the strain energy of the fiber mainly comes from its axial deformation, which is higher than that induced by shape change. Therefore, small values of MFA usually lead to higher strain energy in the fiber-matrix system. However, a relatively large MFA often makes the system more flexible and elastic. This can be used to explain the fact that the towel gourd tendrils usually have the ability to endure large elongation. In addition, it is very easy for slender climbing tendrils to bend to grasp supports.

Helical Fiber Fragmentation

Chiral microstructures, such as helical fibers, usually serve as the main loading-bearing parts of biological composites. Through their deformation and fracture, helical fibrils or fibers effectively contribute to the structural integrity of biological composites. For example, helical fibers transfer stress between crack surfaces and can even be pulled out to dissipate energy, thereby hindering crack propagation and enhancing the fracture toughness of biological composites. If the fiber/matrix interface is large enough, breakage generally occurs before a fiber is pulled out. The previous studies [11] show that biological composites containing helical microstructures can endure larger deformations and dissipate more energy than those with straight fibers, resulting in enhanced fracture toughness. In the following, the helical fiber fragmentation behavior of a fiber-matrix

system undergoing large elongation is investigated using FEM simulation.

In Fig. 4, typical fragmentation processes of helical fibers under different tensile strains are shown. Under applied loading, the fiber helix embedded in the matrix is stretched with nonnegligible axial deformation, and the shear stress of the interface also increases simultaneously for $\varepsilon = 0.27$. When the tensile strain reaches 0.31, the axial stress of the fiber exceeds a critical value, i.e., the fracture strength, and the fiber breaks. In this paper, we use fiber fragment density to describe the degree of failure of the fiber and it refers to the number of broken fibers per unit length. With an increase in tensile strain, shear stress increases and the fiber breaks more. When the tensile strain is $\varepsilon = 0.34$, the fiber fragment density is significantly increased and the fiber breaks into many fragments with curved shapes. At $\varepsilon = 0.38$, the fiber fragment density reaches its maximum and the fiber fragments become straight. At this stage, the interface is fully debonded or the matrix is at complete failure.

The shear stress over the fiber/matrix interface plays an important role in the stress transfer and failure of the fiber-matrix system. Distribution curves of the interfacial shear stress along fiber length for different tensile strains can be seen in Fig. 5. These curves show how the interfacial shear stress is redistributed during fiber fragmentation. Due to the three-dimensional helical geometry, the interfacial shear stress mainly consists of two parts, i.e., tangential shear stress along the axis of the fiber and circumferential stress along its cross-sectional boundary. It is, indeed, difficult to describe completely the complicated spatial distributions of

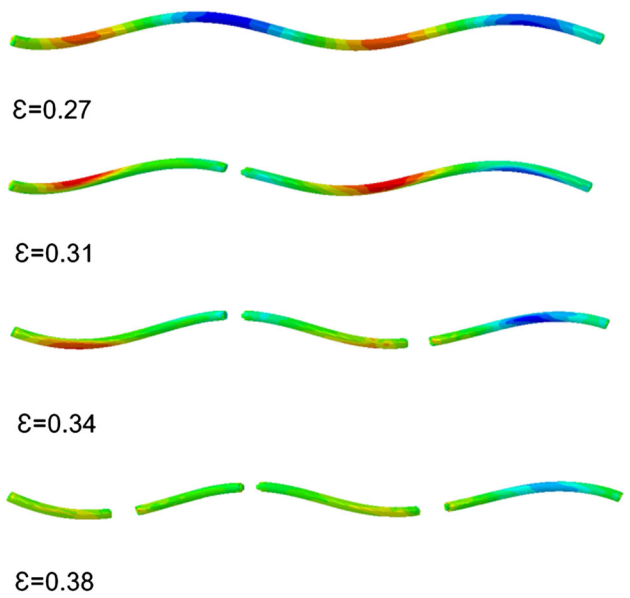

Fig. 4 Fragmentation behavior of helical fibers during loading on a fiber-matrix system with an initial MFA = 45°

interfacial shear stress due to the involvement of multiple coordinate transformations. For simplicity, we describe directly the distribution of interfacial shear stress in a global rectangular coordinate system, as this can basically capture the distribution features. It can be seen from Fig. 5 that the distribution of interfacial shear stress generally takes a periodic wave-like form along the fiber length, induced by the helical shape of the fiber. In Fig. 5, the positive or negative values denote the directions of interfacial shear stress. At the initial loading stage, the interfacial shear stress reaches a high value, leading to fiber breakage. After the fiber is broken into fragments, the interfacial shear stress value degenerates to zero at the points between two neighboring fiber fragments, i.e., breaking points, as shown in Fig. 5b. When the fiber-matrix system is further loaded and the tensile strain of the system increases to a high value such as 0.34 or 0.38, the fiber fragments break into new fragments of much smaller length and the interfacial shear stress is redistributed along the fiber length. Furthermore, the breaking points are usually located at the middle of the previous fiber fragments.

It should be mentioned that the fiber that we considered in Figs. 4 and 5 has two helical periods along its length. Distribution of shear stress exhibits a periodic nature due to the geometric shape of the fiber. To illustrate this, we simulated helical fiber fragmentation behavior in two other cases where the fiber has one and then three helical periods. As shown in Fig. 6, the shear stress along the fiber length distinctly shows a periodic distribution. In addition, the shear stresses along the fiber length after the breaking point also assume a periodic distribution similar to those in Fig. 5 (they are not given here for simplicity). It is noteworthy that due to the end effects and the fact that there are small distances between the ends of the matrix and the fiber, the absolute shear stress values at both ends of the matrix only approximate to each other rather than having the same value. Due to the periodic geometrical shape, we can only consider the case where the fiber has one helical period when investigating fiber fragmentation behavior. The periodic boundary conditions can also be applied to both ends of the matrix.

Figure 7 illustrates variations in fiber fragment density with tensile strain for different initial MFAs. This reveals how the helical shape of microstructures affects the deformation and energy dissipation of biological composites. We consider a typical fiber-matrix system with the initial values of MFA: 0°, 10°, 20°, 30°, and 45°. The results in Fig. 7 show that under small tensile strain, the interfacial shear stress is not high enough to break the fiber and the fiber fragment density equals zero. With an increase in tensile strain, the fiber breaks under the action of interfacial shear stress and the fiber fragment density

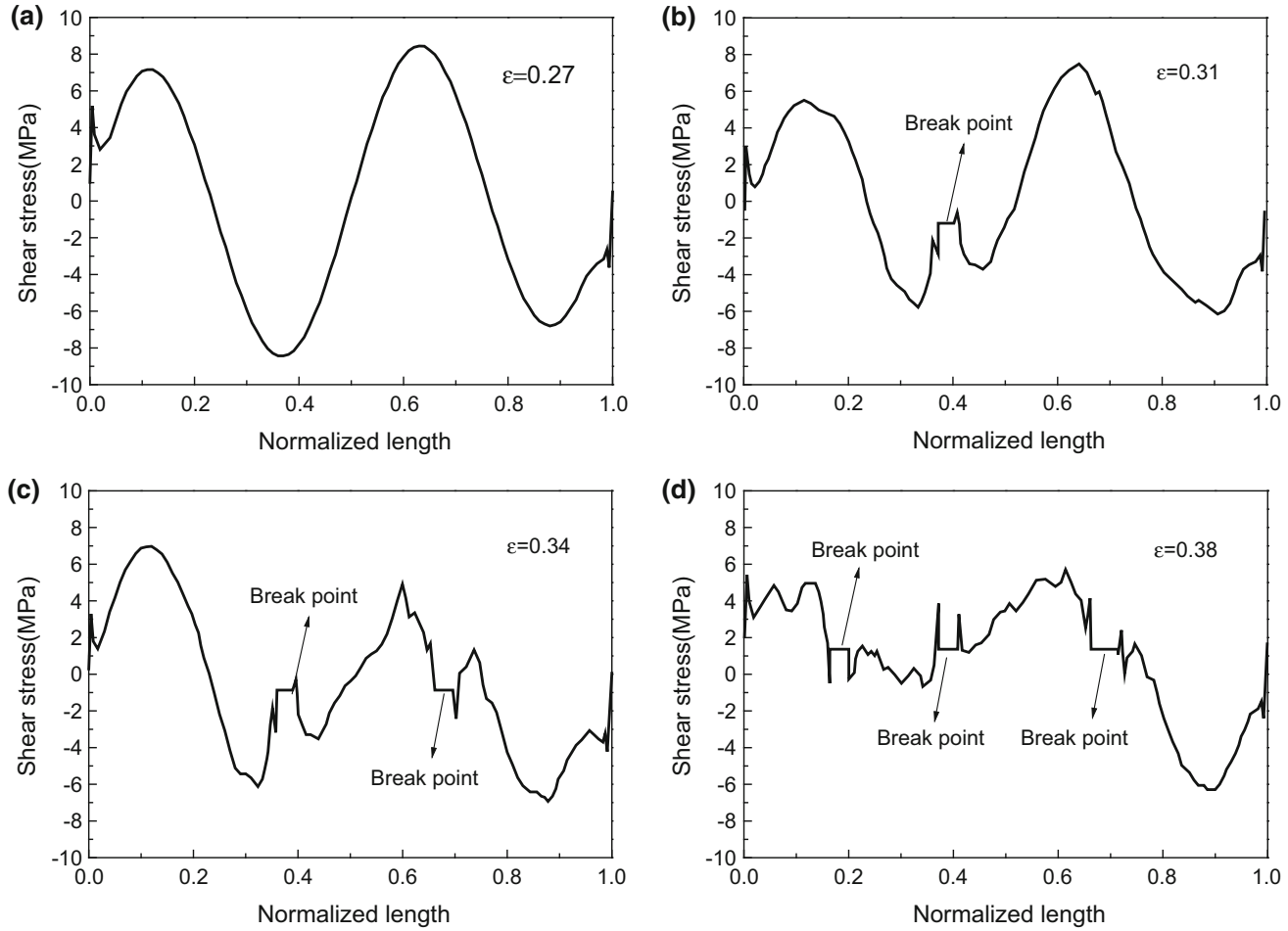

Fig. 5 Distribution of interfacial shear stress along fiber length during helical fiber fragmentation. **a** $\varepsilon = 0.27$, **b** $\varepsilon = 0.31$, **c** $\varepsilon = 0.34$, and **d** $\varepsilon = 038$

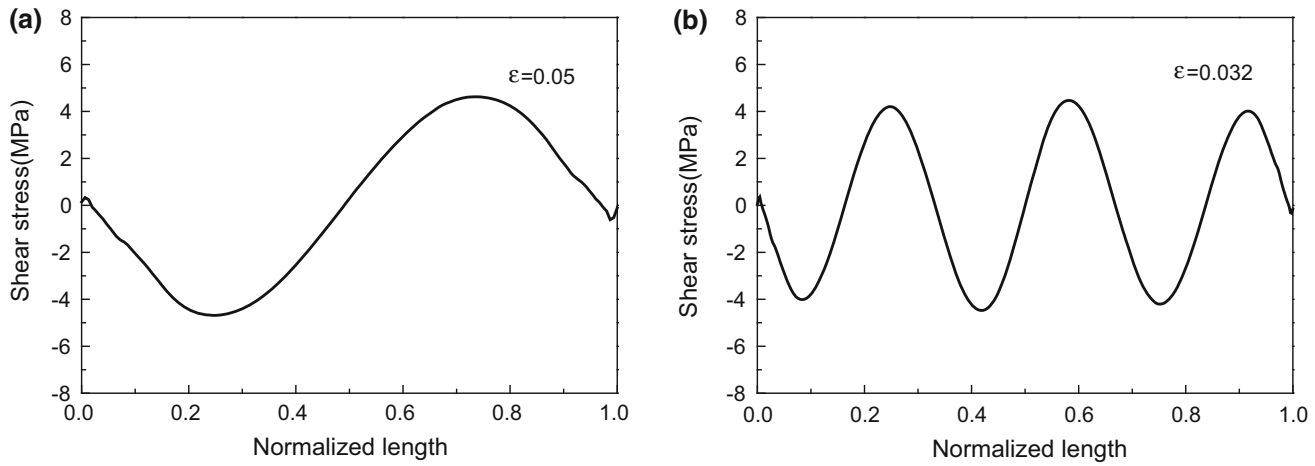

Fig. 6 Distribution of shear stress of fiber along its length during helical fiber fragmentation in the cases that **a** the fiber has one helical period and **b** the fiber has three helical periods

increases linearly up to its maximum. After that, the fiber-matrix system is destroyed completely. At this stage, the fiber-matrix system loses its bearing capacity and the fiber fragment density stays constant rather than increasing. In addition, for a fiber-matrix system with a small initial MFA value, the fiber fragment density is relatively high due to

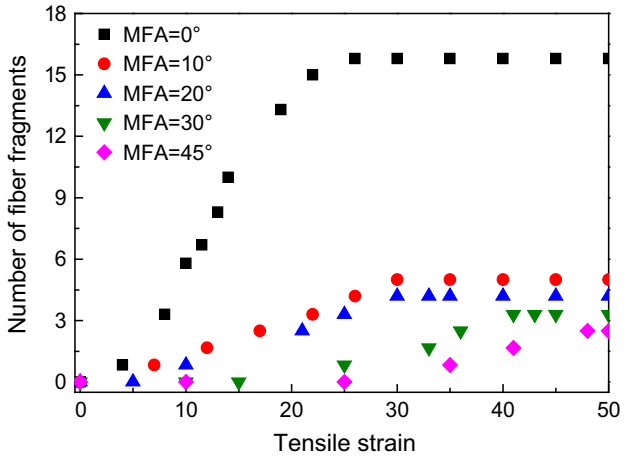

Fig. 7 Effects of different MFA values on fiber fragment density of fiber

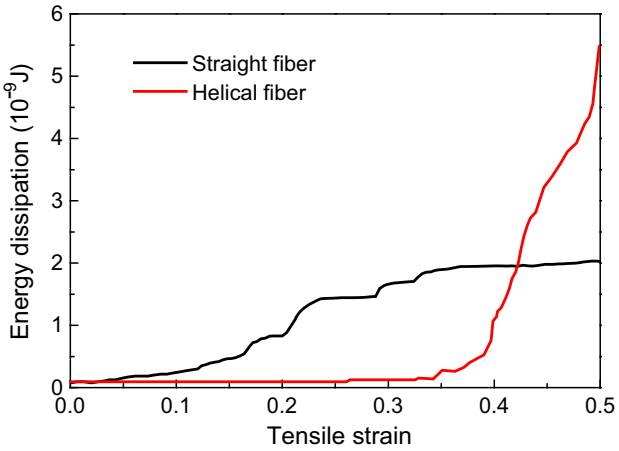

Fig. 8 Variations of dissipation energy of the fiber-matrix system during straight and helical fiber fragmentation processes

the poor capacity of the system to endure large deformation. Relatively large initial MFA values usually induce shape changes in the fiber helix rather than axial deformation of the fiber, endowing the fiber-matrix system with relatively strong capacity to endure large elongation. Therefore, fiber-matrix systems with large initial MFAs have a low fiber fragment density. The results in Fig. 7 demonstrate that the initial helical shape of the fiber can significantly affect the fiber fragment density. When the MFA equals zero, the fiber shape degenerates from a helix to a straight line. As mentioned above, the fragmentation behavior of straight fibers has been extensively investigated [22–24]. Wang et al. [24] conducted a Monte Carlo simulation and experimental tests for the fragmentation process of single carbon T300 fiber composite, based on the elastic–plastic shear-lag theory. Their simulated and experimental results also show that the number of fiber fragments increases linearly with tensile strain, then stays constant at the maximum. Although the elastic–plastic parameters of the fiber considered here are different from those of carbon T300 fibers, the results for the straight fiber in Fig. 7 are consistent, which verifies the simulations in this paper.

To illustrate the effects of the helical shape of a fiber on energy dissipation during fiber fragmentation, variations in dissipation energy with tensile strain for straight and helical fibers are plotted in Fig. 8. During the fiber fragmentation process, energy dissipation is induced by fiber facture, interfacial debonding, matrix crack propagation, and so on. The curves in Fig. 8 show that for a fiber-matrix system with an initial MFA = 30°, shape changes in the fiber helix and deformation of the matrix occur, but no failure of the composite occurs at tensile strains smaller than 0.4. Thus, there is almost no dissipation energy. After a tensile strain of 0.4, the fiber starts to break into fragments and the fiber fragment density increases linearly with the tensile strain. This results in a quick dissipation energy increase correlated with tensile strain. For a fiber-matrix system with a straight fiber, the axial deformation of the fiber becomes large enough when the tensile strain reaches 0.1 and can induce fiber fragmentation. In a unit axial length, a helical fiber is much longer than a straight one due to the three-dimensional periodical geometry. Therefore, a fiber-matrix system with helical fibers usually has much higher dissipation energy than the one with straight fibers at the stage when the fibers are completely broken. The results in Fig. 8 also show that a helical microstructure can enhance the fracture toughness of composites, considering that energy dissipation usually serves as an important origin of toughness.

Conclusions

In this paper, the effects of helical shape of fiber on the deformation and fiber fragmentation process of a fiber-matrix system under large elongation were investigated using FEM. We show that large initial MFA values induce a strong capacity to endure large elongations, which can effectively reduce the chance of fiber fracture. Compared to a straight fiber, the helical shape distinctly increases dissipation energy during fiber fragmentation, suggesting that chiral microstructures can be used to enhance the fracture toughness of composites. This work contributes to the understanding of why so many microstructures in biological materials take chiral shapes such as the helix and twist, and also provides inspiration for the design of advanced composites with high toughness.

Acknowledgements This study was supported by the National Natural Science Foundation of China (Nos. 11472191, 11172207, and 11272230).

References

1. Meyers MA, Chen PY, Lin AYM et al (2008) Biological materials: structure and mechanical properties. Prog Mater Sci 53(1):1–206
2. Shao Y, Zhao HP, Feng XQ et al (2012) Discontinuous crack-bridging model for fracture toughness analysis of nacre. J Mech Phys Solids 60(8):1400–1419
3. Zhao ZL, Zhao HP, Li BW et al (2015) Biomechanical tactics of chiral growth in emergent aquatic macrophytes. Scientific Report 5:12610
4. Ji B, Gao H (2010) Mechanical principles of biological nanocomposites. Annu Rev Mater Res 40(1):77–100
5. Song F, Zhou JB, Xu XH et al (2008) Effect of a negative Poisson ratio in the tension of ceramics. Phy Rev Lett 100(24):245502-1-4
6. Wang JS, Wang G, Feng XQ et al (2013) Hierarchical chirality transfer in the growth of towel gourd tendrils. Sci Rep 3:3102
7. Wang JS, Cui YH, Shimada T et al (2014) Unusual winding of helices under tension. Appl Phys Lett 105(4):043702–043705
8. Neville AC (1993) Biology of fibrous composites: development beyond the cell membrane. Cambridge University, London
9. Zhu HJ, Shimada T, Wang JS et al (2016) Mechanics of fibrous biological materials with hierarchical chirality. J Appl Mech 83(10):101010
10. Zhao ZL, Li B, Feng XQ (2016) Handedness-dependent hyperelasticity of biological soft fibers with multilayered helical structures. Int J Nonlinear Mech 81:19–29
11. Wang LX, Cui YH, Qin QH et al (2016) Helical fiber pull-out in biological materials. Acta Mech Solida Sin 29(3):245–256
12. Liu JL (2013) The analogy study method in engineering mechanics. Int J Mech Eng Educ 41(2):136–145
13. Fratzl P, Misof K, Zizak I et al (1998) Fibrillar structure and mechanical properties of collagen. J Struct Biol 122(1–2):119–122
14. Liu XN, Huang GL, Hu GK (2012) Chiral effect in plane isotropic micropolar elasticity and its application to chiral lattices. J Mech Phys Solids 60(11):1907–1921
15. Lakes RS, Benedict RL (1982) Noncentrosymmetry in micropolar elasticity. Int J Eng Sci 20(10):1161–1167
16. Slepyan L, Krylov V, Parnes R (2000) Helical inclusion in an elastic matrix. J Mech Phys Solids 48(4):827–865
17. Adler DC, Buehler MJ (2013) Mesoscale mechanics of wood cell walls under axial strain. Soft Matter 9(29):7138–7144
18. Chen XY, Beyerlein JI, Brinson LC (2009) Curved-fiber pull-out model for nanocomposites. Part 2: interfacial debonding and sliding. Mech Mater 41(3):293–307
19. Chen YL, Liu B, He XQ et al (2010) Failure analysis and the optimal toughness design of carbon nanotube-reinforced composites. Compos Sci Technol 70(9):1360–1367
20. Fu SY, Zhou BL, Lung CW (1993) On the pull-out of fibres with a branched structure and the inference of strength and fracture toughness of composites[J]. Compos Sci Technol 47(3):245–250
21. Kagawa Y, Nakata E, Yoshida S (1982) Fracture behavior and toughness of helical fiber reinforced composite metals. Progress in science and engineering of composites. ICCM-IV, Tokyo, pp 1457–1464
22. Sørensen BF (2016) Micromechanical model of the single fiber fragmentation test. Mech Mater 104:38–48
23. Lee S, Nguyen T, Chin J et al (1998) Analysis of the single-fiber fragmentation test. J Mater Sci 33(21):5221–5228
24. Wang XH, Zhang B, Du SY et al (2010) Monte Carlo simulation of single fiber composite fragmentation process based on the elastic-plastic shear-lag theory. Acta Mater Compos Sin 27(5):1–6 **(in Chinese)**
25. Hibbit K (1995) Hibbitt, Karlsson & Sorenson, Inc., ABAQUS/Standard Users Manual, i–iii. Karlsson & Sorenson, Inc., USA